Available online at www.sciencedirect.com
ScienceDirect
Remote Sensing of Environment 111 (2007) 357–366
Remote Sensing of Environment
www.elsevier.com/locate/rse

A parameterized multiple-scattering model for microwave emission from dry snow

Lingmei Jiang [a,b,*], Jiancheng Shi [c], Saibun Tjuatja [d], Jeff Dozier [e], Kunshan Chen [f], Lixin Zhang [a,b]

[a] State Key Laboratory of Remote Sensing Science, Jointly Sponsored by Beijing Normal University and the Institute of Remote Sensing Applications of Chinese Academy of Sciences, School of Geography, Beijing Normal University, Beijing, 100875 China
[b] Beijing Key Laboratory for Remote Sensing of Environment and Digital Cities, 100875 China
[c] Institute for Computational Earth System Science, University of California, Santa Barbara, CA 93106-3060, USA
[d] Wave Scattering Research Center, The University of Texas at Arlington, Arlington, TX 76019-0016, USA
[e] Donald Bren School of Environmental Science and Management, University of California, Santa Barbara, CA 93106-5131, USA
[f] Center for Space and Remote Sensing Research, National Central University, 32054 Chung-Li, Taiwan

Received 15 August 2006; received in revised form 20 January 2007; accepted 17 February 2007

Abstract

Snow water equivalent (SWE) is one of the key parameters for many applications in climatology, hydrology, and water resource planning and management. Satellite-based passive microwave sensors have provided global, long-term observations that are sensitive to SWE. However, the complexity of the snowpack makes modeling the microwave emission and inversion of a model to retrieve SWE difficult, with the consequence that retrievals are sometimes incorrect. Here we develop a parameterized dry snow emission model for analyzing passive microwave data, including those from the Advanced Microwave Scanning Radiometer-Earth Observing System (AMSR-E) at 10.65 GHz, 18.7 GHz, and 36.5 GHz for SWE estimation. We first evaluate a multiple-scattering microwave emission model that consists of a single snow layer over a rough surface by comparing model calculations with data from two field measurements, from the Cold Land Process Experiment (CLPX) in 2003 and from Switzerland in 1995. This model uses the matrix doubling approach to include incoherent multiple-scattering in the snow, and the model combines the Dense Media Radiative Transfer Model (DMRT) for snow volume scattering and emission with the Advanced Integral Equation Model (AIEM) for the randomly rough snow/ground interface to calculate dry snow emission signals. The combined model agrees well with experimental measurements. With this confirmation, we develop a parameterized emission model, much faster computationally, using a database that the more physical multiple-scattering model generates. For a wide range of snow and soil properties, this parameterized model's results are within 0.013 of those from the multiple-scattering model. This simplified model can be applied to the simulation of the microwave emission signal and to developing algorithms for SWE retrieval.

Keywords: Radiative transfer; Dry snow; Passive microwave remote sensing; Parameterization

1. Introduction

Characteristics of spatial and temporal distributed snow properties play important roles in global energy and water cycles. Snow cover significantly influences the Earth's surface radiative balance and acts as the frozen storage term in the water balance. Snow water equivalent (SWE) is important for hydrological applications and water resource management. In situ snow cover and SWE data, however, are available only at point measurements in a few areas that are poorly distributed globally (Robinson et al., 1993). Satellite passive microwave imagery has been used as a source of snow cover information because of all-weather imaging capabilities, rapid scene revisit time, and the ability to derive quantitative estimates of SWE (Derksen et al., 2000). Currently, there has been a growing use of microwave radiometry satellite observation in weather and climate prediction model (Marshall et al., 2005). It required

* Corresponding author. School of Geography, Beijing Normal University, Beijing, 100875 PR China. Tel.: +86 10 58809966; fax: +86 10 58805274.
E-mail address: jlingmei@hotmail.com (L. Jiang).

0034-4257/$ - see front matter © 2007 Elsevier Inc. All rights reserved.
doi:10.1016/j.rse.2007.02.034

high accuracy and fast simulations of the satellite observation coupled with forecast modeling. Therefore, the accuracy and efficiency of forecast model is basically linked to both the accuracy and computation time of the radiative transfer model.

Passive microwave remote sensing of snow parameters, such as snow extent, snow water equivalent, and wet/dry state, have been investigated by many researchers using various microwave sensors (Goodison & Walker, 1994; Foster et al., 1997; Derksen et al., 2000; Pulliainen & Hallikainen, 2001, Kelly & Chang, 2003; Roy et al., 2004; Tedesco et al., 2004; Derksen et al., 2005a,b; Macelloni et al., 2005; Pulliainen, 2006). Over a broad range of frequencies, 3–90 GHz, microwave brightness temperature is sensitive to snow crystal characteristics, snow density, and water equivalent (Wiesmann & Mätzler, 1999; Pulliainen et al., 1999; Tsang & Kong, 2001; Macelloni et al., 2001), but it also depends on the physical temperature and properties of the underlying soil. At the lower frequencies, emission from dry snow is mainly affected by underlying soil dielectric and roughness properties; at higher frequencies, emission is sensitive to snow water equivalent and snow particle size since the volume scattering by snow particles becomes important (Mätzler, 1996). Because dry snow emits considerably less microwave radiation than soil, the brightness temperature of snow is inversely related to the snow water equivalent. When snow starts to melt, emission will significantly increase because water droplets absorb and re-emit rather than scatter microwave radiation (Foster et al., 2005).

In recent years, theoretical modeling of microwave emission from snow has advanced significantly and has provided a better understanding of snowpack scattering and emission processes (Mäzler & Wiesmann, 1999; Wiesmann & Mätzler, 1999; Pulliainen et al., 1999; Tsang & Kong, 2001). Snow is a dense medium owing to the high volume fraction of ice grains (10% to 50%), and there are interactions between the emitted microwave signal with the snow volume and surfaces. Snow volume scattering include both coherent (dense medium effect) and incoherent multiple-scattering. Several microwave snow emission models have been reported including the MEMLS model — a multilayer and multiple-scattering radiative transfer model (Wiesmann & Mätzler, 1999; Mäzler & Wiesmann, 1999) and the HUT model (Pulliainen et al., 1999). The dense medium radiative transfer (DMRT) model have been developed for modeling microwave signals of snow cover with either Rayleigh or Mie spherical scattering phase matrices with the quasi-crystalline approximations (Chuah et al., 1996; Tsang et al., 2000; Tsang & Kong, 2001). The DMRT takes into account the coherent wave interactions by the pair distribution function of the particle positions (Percus–Yevick equation) and is suitable for snow application (Tsang & Kong, 2001). The DMRT model predictions are in good agreement with numerical solutions of Maxwell's equations based on three-dimensional simulations (NMM3D), with laboratory controlled measurements (Chen et al., 2003a), and with field measurements for a variety of snow depths, grain sizes and densities (Tsang et al., 2000; Macelloni et al., 2001; Jiang et al., 2004; Tedesco et al., 2006).

Furthermore, theoretical modeling of surface emission and scattering has also significantly improved. The Integral Equation Model (IEM) has demonstrated applicability to a much wider range of surface roughness conditions compared to conventional models. Recently, Chen et al. (2003b) extended the original IEM and developed the Advanced Integral Equation Model (AIEM), by removing some weak assumptions in the original IEM model development. Comparisons of AIEM with NMM3D-simulated data (Chen et al., 2003b) and field experimental data over the frequency range from 6 to 37 GHz (Shi et al., 2005) showed significantly better agreement than the original IEM model over a wide range of surface dielectric, roughness, and sensor frequencies. These efforts have established a fundamentally improved understanding of the effects of snow physical parameters and underlying surface dielectric and roughness properties on the microwave measurements of snow-covered terrain, making it possible to characterize microwave emission more accurately.

Vector radiative transfer theory (VRT), which is based on energy transport of partially polarized electromagnetic waves inside a medium, has been used for studying snow's effects on microwave signatures. A snow-layer emission model based on VRT accounts for incoherent multiple-scattering effects within the layer and the incoherent interactions between the volume and the layer surfaces (Fung, 1994). The VRT equations for a snow layer can be solved numerically using the eigen-analysis technique (Tsang et al., 2000; Tsang & Kong, 2001) or the matrix doubling (MD) method (Ulaby et al., 1986; Tjuatja et al., 1993). In terms of computation, matrix doubling is a more efficient method for layers that are optically thick, as is usual with snow.

By combining the recent advancements of theoretical modeling developments in each scattering and emission components of snow layer and surface with the technique of the multi-scattering radiative transfer solution, it is possible to develop a new multiple-scattering snow emission model that implements the most recent achievements in theoretical model developments to improve our understanding of the effects of the properties of the snow and of the underlying soil. However, a multiple-scattering snow emission model is complex, in general, and makes its direct application for analyses of microwave radiometer data or inferring snow parameters computationally difficult. Therefore, the field needs a simple and accurate snow emission model that can correctly represent the characteristics and relationships of the emission signals, so that a model can be used to drive algorithm development for SWE retrieval by passive microwave remote sensing and to provide a fast dry snow data assimilation model for applications in climate prediction and land surface process modeling affords. The major purpose of this study is to present such a model for terrestrial dry snow cover.

The manuscript is organized as following: In Section 2, we describe a dry snow multiple-scattering microwave emission model that implemented the recent achievements in theoretical model developments for each component. In Section 3, we compare this model with results from two field experiments. In Section 4, we demonstrate the development of a parameterized snow microwave emission model using the simulated data from our dry snow multiple-scattering microwave emission model. Section 5 presents our conclusions.

2. A slab multiple-scattering microwave emission model for dry snow

We have implemented the recent advancements in theoretical model development for both volume and surface emission models. The matrix doubling approach is used to include multiple-scattering and combines the Dense Media Radiative Transfer Model (DMRT) (Tsang, 1992) for snow volume scattering and emission, the Advanced Integral Equation Model (AIEM) for soil emission (Chen et al., 2003b), and the interactions of microwave signals between snow and soil with the surface bistatic scattering model from the AIEM model (Chen et al., 2003b) to calculate dry snow emission. Our multiple-scattering model is a combined DMRT-AIEM-MD microwave emission model for terrestrial dry snow cover with the consideration of one snow layer over a rough soil or rock surfaces.

In VRT formulation, the volume scattering phase matrix characterizes the coupling of intensities in any direction inside the layer caused by scattering and is usually derived using the electromagnetic wave formulation. The volume scattering phase matrix of an optically thin (infinitesimal) layer is determined by the properties of a collection of scatterers. A dry snow layer is a heterogeneous medium composed of ice particles with different sizes and microstructures. The shape and orientation of the snow crystal have little effect on the snow microwave emission (Foster et al., 1999, 2000), so the ice particles can be effectively modeled as spheres. The high volume fraction of ice grains causes the volume scattering to include both coherent scattering (the dense medium effect) and incoherent multiple-scattering. The multiple incoherent scattering is accounted for in the VRT formulation. Several volume scattering models for dense media account for the coherent interactions (Chuah et al., 1996; Tsang et al., 2000; Tsang & Kong, 2001). This study utilizes Tsang and Kong's (2001) volume scattering phase matrix for spatially-correlated spherical scatterers based on the dense medium radiative transfer (DMRT) model with the quasi-crystalline approximation.

Emission of electromagnetic waves from dry snow combines surface and volume scattering. To account for the surface scattering and surface-volume interactions, the VRT equations are subject to the boundary conditions at the air–snow and snow–ground surfaces. In the matrix doubling formulation, these boundary conditions are enforced by including the surface scattering phase matrices (Ulaby et al., 1986; Tjuatja et al., 1993; Fung, 1994). At the air–snow interface, the dielectric contrast between dry snow and air is commonly small, and for emission we neglect surface roughness. Therefore, we consider the air–snow interface as smooth and the snow–ground surface as rough.

To determine the total emission from a snow layer above ground, consider the geometry shown in Fig. 1. The total emission source within a layer can be separated into three components: the total upwelling emission u_u, the total downwelling emission u_d, and the ground emission into the layer u_g. The ground emission u_g is determined by the temperature and emissivity of the soil calculated by AIEM, that depends on the underground soil moisture and roughness at snow–ground

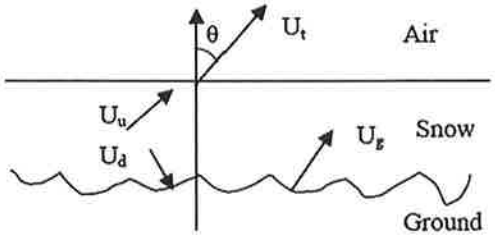

Fig. 1. Geometry of a snow-layer emission problem.

interface. The upwelling and downwelling emissions, u_u and u_d, are functions of the snow-layer temperature profile and its volume scattering properties. For a snow layer with optical thickness τ_0, u_u and u_d are:

$$u_u(\tau_0) = \int_0^{\tau_0} T^0(\tau)\left\{I - \frac{1}{4}S^0(\tau_0-\tau)S^0(\tau)\right\}^{-1}\{I + S^0(\tau_0-\tau)\}(1-a)\frac{K}{\lambda^2}U^{-1}T(\tau)d\tau \quad (1)$$

$$u_d(\tau_0) = \int_0^{\tau_0} T^0(\tau_0-\tau)\left\{I - \frac{1}{4}S^0(\tau)S^0(\tau_0-\tau)\right\}^{-1}\{I + S^0(\tau)\}(1-a)\frac{K}{\lambda^2}U^{-1}T(\tau)d\tau \quad (2)$$

where $S^0(\delta)$ and $T^0(\delta)$ are the zeroth-order Fourier components in the backward and forward scattering phase matrices of the snow layer, they are calculated by the spherical Mie scattering phase matrices with the quasi-crystalline approximation (QCA) and the pair distribution function of the particle positions and coherent wave interactions using Percus–Yevick equation (Tsang & Kong, 2001). I is the identity matrix, U is the directional cosine matrix for the polar angles, K is the Boltzmann constant, T is the temperature profile of the layer, a is the albedo, and λ is wavelength.

The total emission from the snow layer, u_T, is

$$u_T = L_u u_u + L_d u_d + L_g u_g \quad (3)$$

where the L's are multiple-scattering operators that account for all surface and surface-volume multiple-scattering. The volume scattering phase matrices S^0 and T^0 and the multiple-scattering operators L's are solved using the matrix doubling method with the snow/ground boundary conditions computed using AIEM model (Chen et al., 2003a,b) for the surface reflectivity matrix. In this way, the interactions between the scattering and emission from snowpack and the ground rough surface can be taken into account.

3. Comparisons of the model with experimental data

To validate the DMRT-AIEM-MD emission model, we compared the model simulations with two field experimental data sets that were obtained from the ground radiometer measurements over dry snow covers. The first one is from the passive microwave experiments of snowpacks in the Alps (Wiesmann et al., 1996) measured on Dec. 22, 1995 at Weissfluhjoch (46°49, 83′N, 9°48, 62′E) in Davos, Switzerland. The other field experimental data set with both the ground radiometer and snow pit

Table 1
Snow profile data on December 22, 1995 at Weissfluhjoch

Height (m)	Grain Shape	Temperature of snow (°C)	Snow density (kg/m^3)
0.40–0.60	++	−2.2	109.0
0.25–0.40	/\	–	177.0
0.00–0.25	□□	−0.7	259.0

measurements at Fraser (39.9066°N, 105.8829°W) is from the Cold Land Processes Experiment (CLPX) during Feb. 2003 in northern Colorado, U.S.A.

3.1. Comparison with Weissfluhjoch data

In the Weissfluhjoch experiment on 22 Dec 1995, ground radiometric measurements at 11, 35, and 94 GHz were obtained with a set of portable linearly polarized Dicke radiometers, about 160 cm above the surface. The measurements were obtained with incidence angles from 20° to 70° at 5° intervals. Snow properties — collected nearly simultaneously with the radiometric measurements — included snow depth, grain shapes, temperature, permittivity, density and weather conditions. A snow profile was measured with temperature, grain shape, permittivity, and density in 10 cm steps. Permittivity was measured with open coaxial resonators (Mätzler, 1996), and grain shapes were classified according to the international classification for seasonal snow (Colbeck, 1986).The ground is covered with stones and rocks composed of serpentine. The experiment was carried out during a sunny day, with low sky microwave brightness temperatures — 5.7 K, 11.7 K, and 29.0 K at 11, 35 and 94 GHz. The total emissivity (e) of the snowpack observed by the radiometer is

$$e = \frac{T_b - T_{sky}}{T_s - T_{sky}} \tag{4}$$

where T_b, T_s are the observed radiation and snow physical temperature and T_{sky} is the brightness temperature of the downwelling atmospheric radiation.

Table 1 shows the snow profile data (Wiesmann et al., 1996). In a winter snowpack of 60 cm depth, the top layer consists of 20 cm of new snow above a thin crust. Below the crust, the bottom layer consisted of coarse grains. Snow temperature was 271.2 K. The vertical profiles of snow grain shape and density were also available as shown in Table 1. Due to the fact that the DMRT-AIEM-MD model is a one-layer snow model, snow input parameters for the model were a density of 220 kg m^{-3} and a grain radius of 0.4 mm that were determined by fitting the high frequency measurements at 94 GHz because the measurements at 94 GHz cannot "see" the soil surface 60 cm below. There were no observations of the ground surface roughness and soil moisture during the field experiment. The ground surface dielectric and roughness parameters are treated as fitting parameters with the minimum mean square difference between the modeled and the measured brightness temperatures at 11 GHz, where the subsurface emission signals are the dominant emission source. Results are 1 cm of surface rms height and 20 cm of surface correlation length. The ground surface soil dielectric constant was computed using 10% volumetric soil moisture (Dobson et al., 1985).

Fig. 2 shows the observations and the model calculations for vertical and horizontal polarization. At all three frequencies, the DMRT-AIEM-MD model predictions are able to match the measured snow emissivity data reasonably well in terms of magnitudes in both polarizations and in difference between polarizations. Snow emissivity decreases at both v and h polarizations as frequency increases. Similarly, the polarization difference between v and h polarizations also decreases, especially at incidence angle less than 55°. Table 2 summarizes the root mean square error (RMSE) between the model predictions and the measured snow emission data at each frequency. It shows very good agreement in v polarization at all three frequencies with maximum RMSE less than 0.015. However, the results for h polarization are not as good, as with maximum RMSE 0.039. The overall RMSE for all three frequencies is 0.013 for v and 0.033 for h polarization. The reason for the discrepancy between the model and measurements is mainly due to underground signal fitting is poor in h polarization with RMSE 0.038 at X-band, which can result in a poor calculation at Ka-band as shown in Table 2. The other reason might be because the DMRT-AIEM-MD emission model is a slab emission model with the average snow properties from the vertical snow profile, which were taken with a slight adjustment from the high frequency measurements as our model inputs for all frequencies. At lower frequencies, more emission would come from the lower part of the snowpack. The

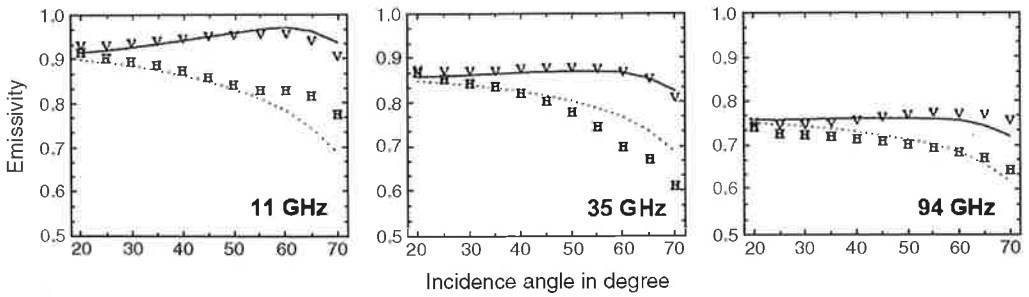

Fig. 2. Emissivity versus incidence angle at 11 GHz, 35 GHz, and 94 GHz. Solid lines show model calculations for vertical polarization, dotted lines for horizontal. Letters represent the corresponding field measurements.

Table 2
RMSE of the comparison of the DMRT-AIEM-MD model with the experiment data on December 22, 1995 at Weissfluhjoch

	Frequency			
Polarization	11 GHz	35 GHz	94 GHz	Overall
v-pol	0.015	0.009	0.015	0.013
h-pol	0.038	0.039	0.015	0.033

underground emission signal might play an important role. At high frequency, however, the underground emission signal might not be significant. The emission signal might mainly come from the upper part of the snowpack due to its limited penetration capability. The simulated emissivity at 94 GHz is very sensitive to snow density, so only a slight change in snow density would result in a significant change in the simulated emissivity. It indicates that the microwave measurements at different frequencies may look at the different snow properties at the different depth depending on its penetration capability. The average snow parameters from the vertical profile measurements may not be the optimal snow parameters for microwave modeling. In addition, the ice lens or a thin crust layer inside the snowpack can considerably affect the spectral behavior of emissivity at the horizontal polarization but not at the vertical polarization (Wiesmann et al., 1998).

3.2. Model comparisons with CLPX'03 data

The Cold Land Process Experiment in 2003 included measurements with the ground-based passive microwave radiometer (GBMR) from the University of Tokyo at three frequencies — 18.7 GHz, 36.5 GHz, and 89 GHz — at both vertical and horizontal polarizations (Graf et al., 2003). The measurement site had an area about 100 m × 100 m at Fraser (39.9066°N, 105.8829°W) in the Rocky Mountains of Colorado. The study area has flat topography and is surrounded by a uniform pine forest and a discontinuous pine forest. Data used in this study were the measurements from dry snow conditions during February 2003. There were two experiment setups, one with a constant incidence angle at 55° and measurements averaged over all azimuths, the other with incidence angles from 30° to 70° but with a fixed azimuth. Each experimental setup was performed at every other day.

During the experiment, there were two light snowfalls on February 20 and 24, and a larger snowfall on 22 February, which added about 20 cm of new fresh snow. Snow pit data were collected around noon from two different snow pit locations within 10 m of the area observed by the radiometer. Faceted crystals were the most plentiful type of ice crystal for this site except on the last day (25 February), when rounded particles and wet agglomerates appeared. This may cause some discrepancy between the real and modeled shapes of ice particles.

The model input parameters were the mean snow depth and density obtained from the ground measurements (Hardy et al., 2003). Snow grain size measurements include the information on minimum, average, and maximum determined by the product of two-dimension optical grain length with a range from about 0.2 mm to 7 mm for each grain size group: small, moderate, and large gain groups. Therefore, the input ice particle size for the model was a fitting parameter selected within the grain size measurement range, which actually was smaller than the observed mean particle size from all measurements. The volumetric soil moisture of 24% measured at 1.5 cm near the site was used to calculate soil dielectric constant (Dobson et al., 1985). It varied little during the entire experiment. The soil roughness properties were the fitting parameters. Since there were no sky brightness temperature observation during this experiment, we calculated T_{sky} for clear-sky conditions (Ulaby et al., 1986; Westwater et al., 1990) at 18.7 GHz, 36.5 GHz and 89 GHz at 18 K, 30 K, and 80 K, respectively. All model input parameters used for simulation are shown in Table 3.

Fig. 3 shows the comparisons between the DMRT-AIEM-MD model emissivities and the measurements. The top plot shows variability with observations angles, and the bottom plot shows a time-series. They show that the predictions of the DMRT-AIEM-MD model compare well with the measurements at the different incidence angles and at all three frequencies. As Table 4, shows the RMSEs are 0.024, 0.019 and 0.017 for *v* polarization and 0.023, 0.022 and 0.009 for *h* polarization at 18.7 GHz, 36.5 GHz, and 89 GHz. Some discrepancies between the measurements and the model calculations exist and can be also explained by the possible reasons as described in analyses of Weissfluhjoch data and model comparison in Section 3.1. For CLPX experimental data, our model performance is better at 36.5 GHz and 89 GHz than at 18.7 GHz. Observed emissivity at 18.7 GHz for both *v* and *h* polarizations increases from 65° to 70° incidence, but at 36.5 GHz and 89 GHz emissivity does not increase. One possible reason might be that the radiometer observed different footprints at difference incidence angles, because the instrument was installed at a fixed height above ground. There may have been different soil properties at the different incidence angles, but these would not affect the signal at the higher frequencies.

Table 3
Averaged snow parameters at Fraser

Date	Feb. 19	Feb. 20	Feb. 21	Feb. 22	Feb. 23	Feb. 24	Feb. 25
Depth (m)	0.80	0.83	0.78	1.02	0.99	1.08	0.99
Density (kg/m^3)	227	228	204	202	206	212	214
Radius (mm)	0.38	0.39	0.36	0.35	0.34	0.33	0.33
T_{snow} (°C)	−2.0	−2.0	−1.0	−0.0	−3.0	−3.0	−2.0
T_{ground} (°C)	−0.0	−0.0	−0.0	−0.0	−0.0	−1.0	−0.0

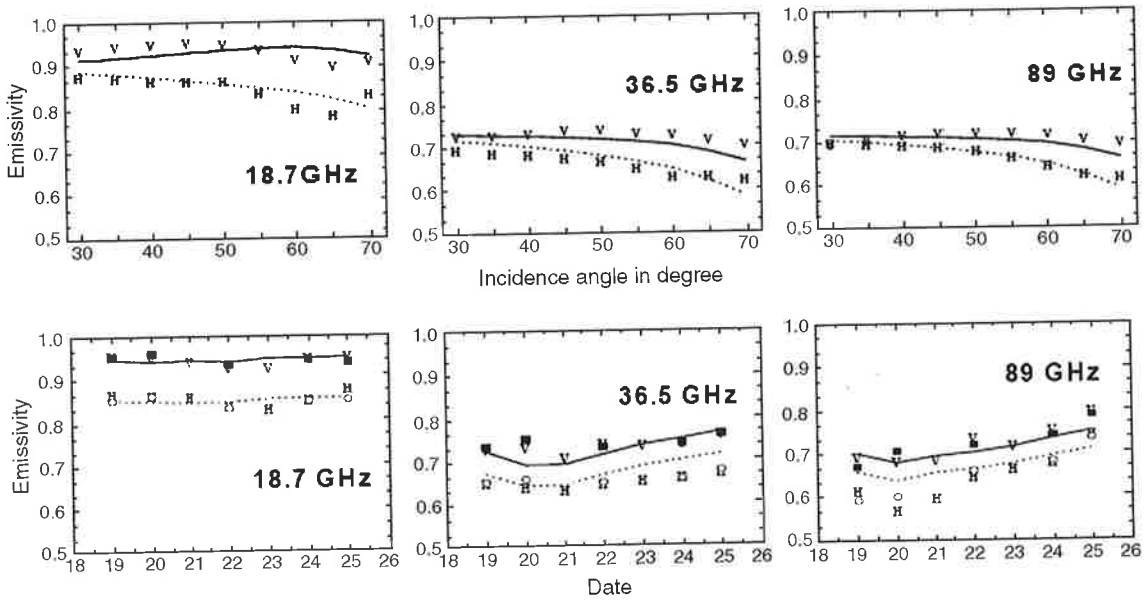

Fig. 3. Comparison of the model with observation at different angles (bottom) on 22 Feb 2003 (top) and with time-series observation at 55° incidence angle from 19–25 Feb 2003 (bottom). Solid and dotted lines show model calculations for v and h polarization. Letters show the measurements.

In the time-series observations, RMSEs are 0.011, 0.023 and 0.024 for v polarization and 0.013, 0.031 and 0.04 for h polarization at 18.7 GHz, 36.5 GHz, and 89 GHz, respectively (Table 4). The significant jump in the 89 GHz observations on 25 Feb is probably caused by melting snow in the surface layer.

Recognizing there are also uncertainties in the field data, we believe that the model and observations agree reasonably well.

4. Development of a parameterized model

At low frequencies, the commonly used ω–τ model is derived from the analytical solution of the 0th-order radiative transfer equations. Without considering snow and ground temperature, total emissivity E_p^t is

$$E_p^t = \left(E_p^v + E_p^v \cdot L_p \cdot R_p^c + L_p \cdot E_p^s\right) \cdot \Psi_p \tag{5}$$

The superscripts t, v, and s represent the emissivity components for total, volume, and surface. The subscript p represents the polarization status v or h. ψ is the power transmittivity at the air–snow interface. $L_p=\exp(-\tau/\cos(\theta_r))$ is the attenuation factor. θ_r is the refractive angle in the snow layer and τ is snow optical thickness. $R_p^c=1-E_p^s$ is the ground surface effective reflectivity. Eq. (5) is commonly considered as a three-component model. The first term is the direct snow emission component $E_p^v=(1-\omega)\cdot(1-L_p)$ where ω is the snow volume scattering albedo. The second term in Eq. (5) is the snow–ground interaction term and represents that the downward snow emission signal is reflected back through the snow layer again. The last term in Eq. (5) represents the underground emission signal after passing through snowpack.

The 0th-order and 1st-order radiative transfer models cannot predict emission very well when the snow volume scattering albedo and optical thickness are large (Ulaby et al., 1986; Fung, 1994). They commonly underestimate snow emission signals. On the other hand, the multiple-scattering snow emission model is very complex, without an analytic solution, and computationally intensive. It is unrealistic to apply the multiple-scattering model directly in analyses of satellite measurements and for SWE algorithm development. Therefore, it is necessary to develop a simple but accurate dry snow emission model that can be used for both fast forward simulation and development of SWE inversion models. To avoid the weakness of some empirical approaches, we use a database generated by the multiple-scattering model that covers most possible snow and soil surface conditions. For specifications of a simple model, we have adopted the following constraints:

- The model must be accurate at each frequency and polarization that is used in the remote sensing application.
- The model must use the snow's physical characteristics, as indicated by the simple radiative transfer model.

Although the low scattering-order models such as 0th-order or 1st-order radiative transfer models that do not take multiple-scattering into account, they provide basic descriptions of the characteristics of microwave emission signal in responding to snow and soil properties. They are valid when snow scattering

Table 4
RMSE of the comparisons of the DMRT-AIEM-MD model with the experiment data at Fraser

	Frequency			
Polarization	18 GHz	36 GHz	89 GHz	Overall
v-pol (time-series)	0.011	0.023	0.024	0.0205
h-pol (time-series)	0.013	0.031	0.040	0.030
v-pol (angular)	0.024	0.019	0.017	0.020
h-pol (angular)	0.023	0.022	0.009	0.019

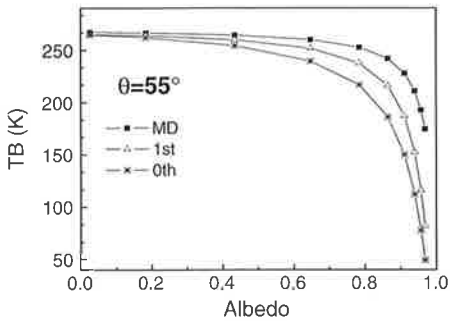

Fig. 4. Emission comparison for different scattering-order solutions at 55° incidence angle at vertical polarization (MD — matrix doubling method, 1st — first-order solutions, 0th — the zeroth-order solutions).

albedo and optical thickness are not too large. For large snow albedo and optical thickness, the low scattering-order models underestimate the emission signals, as Fig. 4 shows. The simulated emissivities by the different scattering-order models clearly show the same trend, i.e., the emission signal decreases as the scattering albedo increases. Although the 0th-order radiative transfer model underestimates the brightness temperature, it is possible to select this model as the basic form and add corrections to include multiple-scattering for our parameterized dry snow emission model.

To start, we simulated dry snow emission for both v and h polarizations at an incident angle of 55° using our DMRT-AIEM-MD model, using AMSR-E frequencies 10.65 GHz, 18.7 GHz, and 36.5 GHz. The simulations cover a wide range of snow and soil dielectric and roughness values as summarized in Table 5. The commonly used Gaussian correlation function for the soil surface was used in the simulation since it is a better approximation for high frequency microwave measurements than the exponential correlation function. With the different combinations of each snow and ground parameter, there are 153,600 DMRT-AIEM-MD model simulated emissivities at each frequency and polarization.

The 0th-order radiative transfer model (4) can be rearranged to a two-component model as

$$E_p^t = \left(E_p^v \cdot (1+L_p) + L_p \cdot \left(1-E_p^v\right) \cdot E_p^s\right) \cdot \Psi_p = \left(\text{Intercept} + \text{slope} \cdot E_p^s\right) \cdot \Psi_p \quad (6)$$

The total emission and soil emission signals can be described as a linear function with the slope and intercept that depend only on snowpack emission and attenuation properties or that are affected only by snow properties. Based on this description, we first divided the DMRT-AIEM-MD model simulated emissivity by the power transmissivity Ψ_p, then carried out the linear regression analyses between a set of all simulated ground surface emission signals and the corresponding total emission signals for a given snow grain size and density. In this way, the linear regression coefficients represent the snowpack emission and attenuation properties with the multiple-scattering effects for that snow grain size and density. By looping through different combinations of snow grain size and density in the ranges as listed in Table 5, all slopes and intercepts can be determined for all snow grain sizes and densities. Unfortunately, this technique can be only applied to the conditions when the soil emission signals can penetrate the snowpack. Therefore, we limit our analyses to the data with snow optical thickness $\tau \leq 2$ at each frequency in our simulated database.

Through our analyses and comparison with the components of the 0th-order radiative transfer model, we develop our parameterized dry snow emission model that includes multiple-scattering:

$$E_{mp}^t \approx \left(E_p^v \cdot Cf_p^v + L_p \cdot \left(1-E_p^v\right) \cdot Cf_p^{svs} E_p^s\right) \cdot \Psi_p \quad (7)$$

E_{mp}^t is the total emissivity simulated by our multiple-scattering model. The first term $E_p^v \cdot Cf_p^v$ is the intercept determined in the linear regression analyses. E_p^v is direct snow volume emissivity in the 0th-order form as given in Eq. (5).Cf_p^v is the multiple-scattering correction factor that corrects for the difference in the direct volume emission signal between the 0th-order and the multiple-scattering models:

$$Cf_p^v = a + b \cdot \omega + \tau' \cdot \left(c + d \cdot \omega + e \cdot \omega^2\right) \quad (8)$$

where $\tau' = \tau/\cos(\theta_t)$ is the optical path length and where the coefficients a, b, c, d and e are determined by the linear regression analysis and are given in Table 6.

The second term in Eq. (7), excluding the underground emissivity E_p^s, L_p $(1-E_p^v)$ Cf_p^{svs} represents the slopes determined

Table 5
Snow and ground parameters for the database simulation

Input parameters	Minimum	Maximum	Step	Units
Snow density	150	450	100	Kg m^{-3}
Grain radius	0.2	1.6	0.2	Mm
Snow depth	0.1	2.0	0.1	m
Ground rms height	0.5	3.0	0.5	cm
Ground surface rms slope	0.05	0.25	0.05	–
Soil moisture	5	40	5	%

Table 6
Coefficients in Eq. (8) for calculating Cf_p^v

Frequency (GHz)	a	b	c	d	e
10.7	2.098563	−0.8514113	0.07340312	0.4980226	−1.874751
18.7	2.112606	−0.8829258	0.108098	0.5742384	−1.279307
36.5	2.120885	−0.7705214	0.07772004	0.3342744	−1.280769

Table 7
Coefficients in Eq. (9) for calculating Cf_p^{svs}

Frequency (GHz)	A	B	C	D
10.7	−0.0268096	0.43702293	0.89230177	−0.75151270
18.7	−0.0737394	0.52525146	0.71524232	−0.61666468
36.5	−0.1397970	0.6268216	0.5559191	−0.4737233

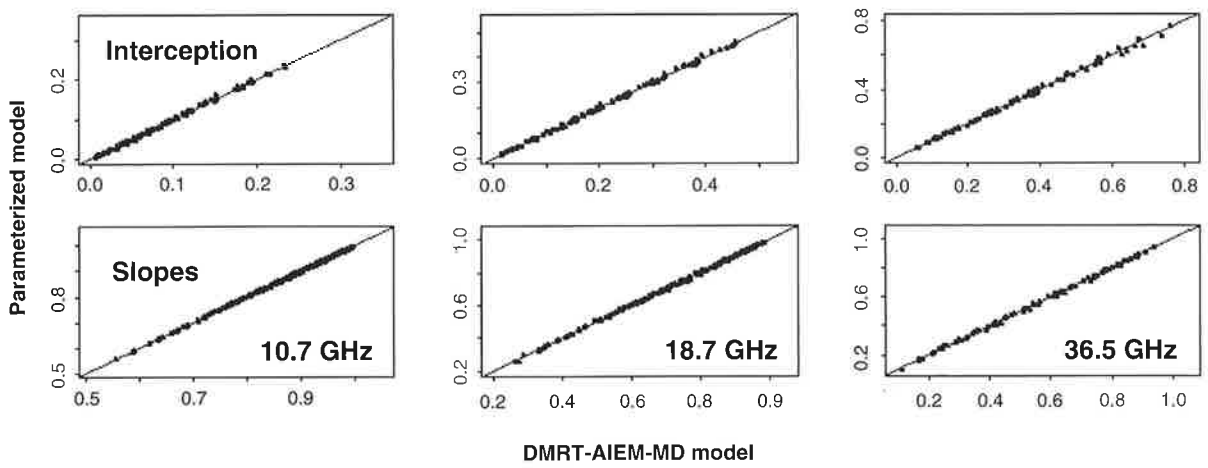

Fig. 5. Comparison of the interceptions (top row) and slopes (bottom row) determined by the DMRT-AIEM-MD model simulated data and these modeled by (7) for frequencies of 10.7, 18.7, and 36.5 GHz from left to right.

by the linear regression analyses. The multiple-scattering correction factor Cf_p^{svs} can be expressed as

$$Cf_p^{svs} = \exp\left[\tau' \cdot (A + B \cdot \omega) + \tau'^2 \cdot \left(C \cdot \omega + D \cdot \omega^2\right)\right] \quad (9)$$

Similarly, the coefficients A, B, C, and D are constants determined by regression analysis, given in Table 7.

Fig. 5 (top row) shows the comparisons between the intercepts that were determined by the linear regression analyses and the model for the first term in Eq. (7): $E_p^v \cdot Cf_p^v$. The differences between these two are extremely small with RMSEs of 0.0017, 0.0033, and 0.007 for 10.65, 18.7, and 36.5 GHz, respectively. Fig. 5 (bottom row) shows the comparisons between the slopes that were determined by the linear regression analyses and the model in the second term of Eq. (7): $L_p\ (l - E_p^v)\ Cf_p^v$. Similarly, the errors are also very small with RMSEs of 0.0015, 0.0039 and 0.0081 for 10.65, 18.7, and 36.5 GHz, respectively.

Fig. 6 (top row) shows the comparisons between the DMRT-AIEM-MD model simulated emissivities and the simple parameterized model for v polarization at 10.65, 18.7, and 36.5 GHz. The bottom row in Fig. 6 shows these for h polarization. The differences between these two models are extremely small with RMSEs of 0.0041, 0.0071, and 0.010 for v polarization at the frequencies of 10.65, 18.7, and 36.5 GHz, respectively. These for h polarization are 0.0052, 0.0087, and 0.013 at 10.65, 18.7, and 36.5 GHz. This simple parameterized model approaches the complex multiple-scattering model fairly well. The RMSEs at 10.7 GHz are the smallest among these three frequencies because multiple-scattering at lower frequency is smaller than that at higher frequencies. From these comparisons, the errors resulted in Eqs. (7–9) are not significant. The simple parameterized model provides both a fast way to simulate dry snow emission signals and a future possibility for improving algorithms for remote sensing of snow water equivalent. The newly developed dry snow emission model Eq. (7) is very simple and suitable for the microwave remote sensing applications with the negligible error in comparison to the complex multiple-scattering model simulations.

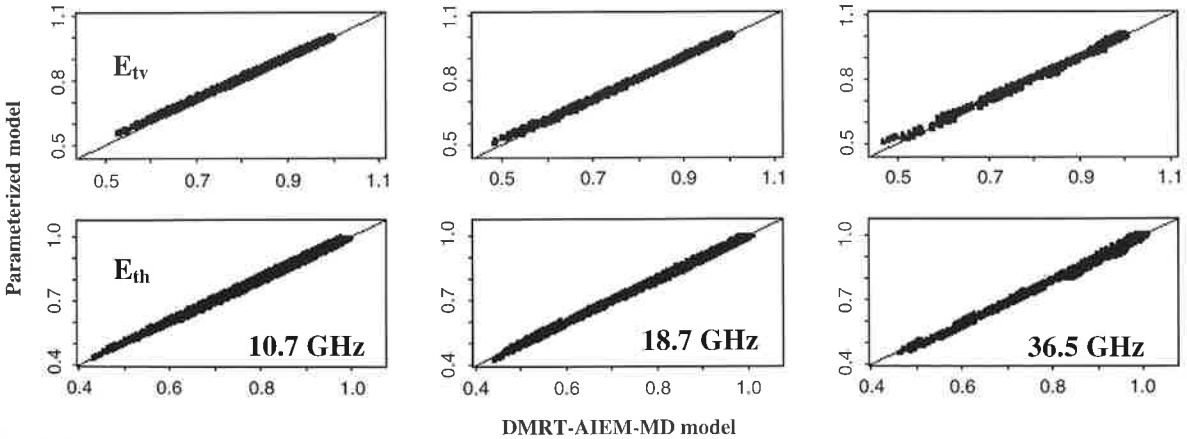

Fig. 6. Comparison of the total emissivities calculated by the DMRT-AIEM-MD model simulated data and these modeled by (7) for v polarization (top row) and h polarization (bottom row) at the frequencies of 10.7, 18.7, and 36.5 GHz from left to right.

5. Conclusions

The recent improvements in both volume and surface scattering models have made it possible to simulate dry snow emission signals for a very wide range of snow and soil conditions. We have integrated these recent developments into the DMRT-AIEM-MD emission model to simulate dry snow microwave emission with multiple-scattering. Comparisons with field data at Weissfluhjoch and CLPX'03 show good agreement for all frequencies and both polarizations.

With confirmed confidence in our multiple-scattering snow emission model, we develop a parameterized multi-frequency-polarization dry snow emission model for fast simulation and analyses of the passive microwave satellite measurements from AMSR-E. This model has a simple form similar to the 0th-order radiative model but adjusted with multiple-scattering correction factors. The differences between the simple parameterized model and the multiple-scattering model DMRT-AIEM-MD are extremely small, with the RMSEs in 10^{-3} range for all three study frequencies at 10.65, 18.7, and 36.5 GHz and both v and h polarizations, except the RMSE is 0.013 at 36.5 GHz and h polarization. This simple model provides a simple, accurate connection between dry snow emission at different frequencies and polarizations. It can be applied to the conditions with the snow optical thickness $\tau \leq 2$ at each of the three studied frequencies and with the dielectric homogeneous half space underground. The simple dry snow emission model developed in this study should be useful in understanding and analyzing the current and past passive microwave satellite measurements of the fully snow-covered pixels. In global SWE monitoring, however, the sub-grid heterogeneity is expected to have the significant impact and has to be taken into account. This issue needs to be further studied.

Acknowledgements

This work was supported by the National Natural Science Foundation of China (90302008), by the NASA NNG04GC52A and by Program for Changjiang Scholars and Innovative Research Team in University (PCSIRT). The two sets of ground field data used in this study were obtained from Snow Tools Signature Database and from CLPX data at National Snow and Ice Data Center (NSIDC). We also thank the anonymous reviewers for their helpful comments on this paper.

References

Chen, C. T., Tsang, L., Guo, J., Chang, A. T. C., & Ding, K. H. (2003). Frequency dependence of scattering and extinction of dense media based on three-dimensional simulations of Maxwell's equations with applications to snow. *IEEE Transactions on Geoscience and Remote Sensing*, *41*(8), 1844–1852.

Chen, K. S., Wu, T. -D., Tsang, L., Li, Q., Shi, J., & Fung, A. K. (2003). Emission of rough surfaces calculated by the integral equation method with comparison to three-dimensional moment method simulations. *IEEE Transactions on Geoscience and Remote Sensing*, *41*(1), 90–101. doi:10.1109/TGRS.2002.807587

Chuah, H. -T., Tjuatja, S., Fung, A. K., & Bredow, J. W. (1996). A phase matrix for a dense discrete random medium: Evaluation of volume scattering coefficient. *IEEE Transactions on Geoscience and Remote Sensing*, *34*(5), 1137–1143. doi:10.1109/36.536529

Colbeck, S. C. (1986). Classification of seasonal snow cover crystals. *Water Resources Research*, *22*(9, suppl.), 59S–70S.

Derksen, C., LeDrew, E., Walker, A., & Goodison, B. (2000). Influence of sensor overpass time on passive microwave-derived snow cover parameters. *Remote Sensing of Environment*, *71*, 297–308.

Derksen, C., Walker, A., Goodison, B., & Walter, S. (2005). Integrating in situ and multiscale passive microwave data for estimation of subgrid scale snow water equivalent distribution and variability. *IEEE Transactions on Geoscience and Remote Sensing*, *43*(5), 960–972.

Derksen, C., Walker, A., & Goodison, B. (2005). Evaluation of passive microwave snow water equivalent retrievals across the boreal forest/tundra transition of western Canada. *Remote Sensing of Environment*, *96*, 315–327.

Dobson, M. C., Ulaby, F. T., Hallikainen, M. T., & El-Reyes, M. (1985). Microwave dielectric behavior of wet soil, part 2: Dielectric mixing models. *IEEE Transactions on Geoscience and Remote Sensing*, *23*, 35–46.

Foster, J. L., Chang, A. T. C., & Hall, D. K. (1997). Comparison of snow mass estimates from prototype passive microwave snow algorithm, a revised algorithm and a snow depth climatology. *Remote Sensing of Environment*, *62*(2), 132–142. doi:10.1016/S0034-4257(97)00085-0

Foster, J. L., Hall, D. K., Chang, A. T. C., Rango, A., Wergin, W., & Erbe, E. (1999). Effects of snow crystal shape on the scattering of passive microwave radiation. *IEEE Transactions on Geoscience and Remote Sensing*, *37*(2), 1165–1168. doi:10.1109/36.752235

Foster, J. L., Barton, J. S., Chang, A. T. C., & Hall, D. K. (2000). Snow crystal orientation effects on the scattering of passive microwave radiation. *IEEE Transactions on Geoscience and Remote Sensing*, *38*(5), 2430–2434.

Foster, J. L., Sun, C., Walker, J. P., Kelly, R. E. J., Chang, A. T. C., Donga, J., et al. (2005). Quantifying the uncertainty in passive microwave snow water equivalent observations. *Remote Sensing of Environment*, *94*(2), 187–203. doi:10.1016/j.rse.2004.09.012

Fung, A. K. (1994). *Microwave Scattering and Emission Models and their Applications* (pp. 573). Boston: Artech House.

Goodison, B., & Walker, A. (1994). Canadian development and use of snow cover information from passive microwave satellite data. In B. Choudhury, Y. Kerr, E. Njoku, & P. Pampaloni (Eds.), *Passive Microwave Remote Sensing of Land-Atmosphere Interactions* (pp. 245–262). Utrecht: VSP BV.

Graf, T., Koike, T., Fujii, H., Brodzik, M., & Armstrong, R. (2003). CLPX-ground: Ground Based Passive Microwave Radiometer (GBMR-7) Data. *National Snow and Ice Data Center* : Boulder, CO.

Hardy, J., Pomeroy, J., Link, T., Marks, D., Cline, D., Elder, K., et al. (2003). Updated 2003 CLPX-Ground: Snow measurements at the Local Scale Observation Site (LSOS). National Snow and Ice Data Center: Boulder, CO.

Jiang, L., Shi, J., Tjuatja, S., & Chen, K. S. (2004). *A comparison of dry snow emission model with field observations. Proceedings IGARSS 2004, Vol. 6* (pp. 3709–3712). doi:10.1109/IGARSS.2004.1369926

Kelly, R. E. J., & Chang, A. T. C. (2003). Development of a passive microwave global snow depth retrieval algorithm for Special Sensor Microwave Imager (SSM/I) and Advanced Microwave Scanning Radiometer-EOS (AMSR-E) data. *Radio Science*, *38*(4), 8076. doi:10.1029/2002RS002648

Macelloni, G., Paloscia, S., Pampaloni, P., & Tedesco, M. (2001). Microwave emission from dry snow: a comparison of experimental and model results. *IEEE Transactions on Geoscience and Remote Sensing*, *39*(12), 2649–2656. doi:10.1109/36.974999

Macelloni, G., Paloscia, S., Pampaloni, P., Brogioni, M., Ranzi, R., & Crepaz, A. (2005). Monitoring of melting refreezing cycles of snow with microwave radiometers: The Microwave Alpine Snow Melting Experiment (MASMEx 2002–2003). *IEEE Transactions on Geoscience and Remote Sensing*, *43*(11), 2431–2442.

Mätzler, C. (1996). Microwave permittivity of dry snow. *IEEE Transactions on Geoscience and Remote Sensing*, *34*(2), 573–581. doi:10.1109/36.485133

Mäzler, C., & Wiesmann, A. (1999). Extension of the microwave emission model of layered snowpacks to coarse-grained snow. *Remote Sensing of Environment*, *70*, 317–325.

Marshall, J. L., Weng, F., Lord, S., Riishojgaard, L., Phoebus, P., & Yoe, J. (2005). Recent advances at the joint center for satellite data assimilation.

Ninth Symposium on Integrated Observing and Assimilation Systems for the Atmosphere, Oceans, and Land Surface (IOAS-AOLS).

Pulliainen, J. T., Grandell, J., & Hallikainen, M. T. (1999). HUT snow emission model and its applicability to snow water equivalent retrieval. *IEEE Transactions on Geoscience and Remote Sensing, 37*(3), 1378–1390. doi:10.1109/36.763302

Pulliainen, J., & Hallikainen, M. (2001). Retrieval of regional snow water equivalent from space-borne passive microwave observations. *Remote Sensing of Environment, 75*, 76–85.

Pulliainen, J. (2006). Mapping of snow water equivalent and snow depth in boreal and sub-arctic zones by assimilating space-borne microwave radiometer data and ground-based observations. *Remote Sensing of Environment, 101*, 257–269.

Robinson, D. A., Dewey, K. F., & Heim, R. R. (1993). Global snow cover monitoring: an update. *Bulletin of the American Meteorological Society, 74*, 1689–1696.

Roy, V., Goita, K., Royer, A., Walker, A. E., & Goodison, B. E. (2004). Snow water equivalent retrieval in a Canadian boreal environment from microwave measurements using the HUT snow emission model. *IEEE Transactions on Geoscience and Remote Sensing, 42*(9), 1850–1859. doi:10.1109/TGRS.2004.832245

Shi, J., Jiang, L., Zhang, L., Chen, K. -S., Wigneron, J. -P., & Chanzy, A. (2005). A parameterized multifrequency-polarization surface emission model. *IEEE Transactions on Geoscience and Remote Sensing, 43*(12), 2831–2841. doi:10.1109/TGRS.2005.857902

Tedesco, M., Pulliainen, J., Takala, M., Hallikainen, M., & Pampaloni, P. (2004). Artificial neural network-based techniques for the retrieval of SWE and snow depth from SSM/I data. *Remote Sensing of Environment, 90*, 76–85.

Tedesco, M., Kim, E. J., Cline, D., Graf, T., Koike, T., Armstrong, R., et al. (2006). Comparison of local scale measured and modeled brightness temperatures and snow parameters from the CLPX 2003 by means of a dense medium radiative transfer theory model. *Hydrological Processes, 20*(4), 657–672. doi:10.1002/hyp.6129

Tjuatja, S., Fung, A. K., & Dawson, M. S. (1993). An analysis of scattering and emission from sea ice. *Remote Sensing Reviews, 7*, 83–106.

Tsang, L. (1992). Dense media radiative transfer theory for dense discrete random media with particles of multiple sizes and permittivities. *Progress in Electromagnetic Research, 6*(5), 181–225.

Tsang, L., Kong, J. A., & Ding, K. -H. (2000). Scattering of electromagnetic waves. *Theories and Applications.* New York: Wiley-Interscience 445 pp.

Tsang, L., & Kong, J. A. (2001). Scattering of electromagnetic waves. *Advanced Topics.* New York: Wiley-Interscience. 432 pp.

Ulaby, F. T., Moore, R. K., & Fung, A. K. (1986). *Microwave Remote Sensing: Active and Passive, from Theory to Applications.* Boston: Artech House 1120 pp.

Wiesmann, A., Stozzi, T., & Weise, T. (1996). *Passive microwave signature catalogue of snowcovers at 11, 21, 35, 48 and 94 GHz. IAP Research Report, Vol. 96–8. University of Bern.*

Wiesmann, A., Mätzler, C., & Weise, T. (1998). Radiometric and structural measurements of snow samples. *Radio Science, 33*(2), 273–289.

Wiesmann, A., & Mätzler, C. (1999). Microwave emission model of layered snowpacks. *Remote Sensing of Environment, 70*, 307–316.

Westwater, E. R., Snider, J. B., & Falls, M. J. (1990). Ground-based radiometric observations of atmospheric emission and attenuation at 20.6, 31.65, and 90.0 GHz: A comparison of measurements and theory. *IEEE Transactions on Antennas and Propagation, 38*(10), 1569–1580. doi:10.1109/8.59770